Transplantation and Cellular Therapy 32 (2026) 454–465

Transplantation and Cellular Therapy

journal homepage: www.astctjournal.org

ASTCT American Society for Transplantation and Cellular Therapy

Full Length Article
Allogeneic – Adult

Spatial Transcriptomics Analysis of Macrophage-to-Myofibroblast Transition in Bronchiolitis Obliterans Following Hematopoietic Stem Cell Transplantation

Akira Yamamoto[1,2], Nobuharu Fujii[1,3,*], Keisuke Seike[1], Seiichiro Sugimoto[4], Yusuke Naoi[5,6], Tomohiro Nagano[6], Saya Kubota[6], Yui Kambara[2,7], Kanako Fujiwara[6], Toshiki Terao[6], Tadashi Oyama[6], Mari Kunihiro[6], Hiroki Kobayashi[1], Takumi Kondo[1], Hideaki Fujiwara[1], Noboru Asada[1], Daisuke Ennishi[1,5], Keiko Fujii[1,8], Shinichi Toyooka[9], Yoshinobu Maeda[1]

[1] *Department of Hematology and Oncology, Okayama University Hospital, Okayama, Japan*
[2] *Dan L Duncan Comprehensive Cancer Center, Baylor College of Medicine, Houston, Texas*
[3] *Division of Transfusion and Cell therapy, Okayama University Hospital, Okayama, Japan*
[4] *Department of General Thoracic Surgery and Organ Transplant Center, Okayama University Hospital, Okayama, Japan*
[5] *Center for Comprehensive Genomic Medicine, Okayama University Hospital, Okayama, Japan*
[6] *Department of Hematology, Oncology and Respiratory Medicine, Okayama University Graduate School of Medicine, Dentistry and Pharmaceutical Sciences, Okayama, Japan*
[7] *Department of Hematology, Oncology and Respiratory Medicine, Okayama University Medical School, Okayama, Japan*
[8] *Division of Clinical Laboratory, Okayama University Hospital, Okayama, Japan*
[9] *Department of General Thoracic Surgery and Breast and Endocrinological Surgery, Faculty of Medicine, Dentistry and Pharmaceutical Science, Okayama University Graduate School of Medicine, Dentistry and Pharmaceutical Sciences, Okayama, Japan*

Article history:
Received 13 August 2025
Accepted 10 December 2025

Key Words:
Bronchiolitis obliterans
GeoMx
Graft versus host disease
Hematopoietic stem cell transplantation
Macrophage

A B S T R A C T

Bronchiolitis obliterans (BO) is a severe, fibrotic manifestation of chronic graft-versus-host disease (GVHD) after hematopoietic stem cell transplantation (HSCT). Macrophage-derived TGF-β is linked to GVHD-related fibrosis; however, its role in BO remains unclear. Given emerging evidence of macrophage-to-myofibroblast transition (MMT) in fibrosis, this study aimed to investigate whether MMT contributes to BO development. We analyzed lung samples from 3 HSCT recipients with BO who underwent lung transplantation, with tissues from 2 patients with lung cancer as controls. Immunofluorescent staining for CD68, CD206, and α-SMA was used to identify cells undergoing MMT. Spatial transcriptomics was performed to profile gene expression in foamy macrophages across anatomical regions and histological stages, compared to control peribronchiolar regions.

Abbreviations: α-SMA, Alpha-smooth muscle actin; ACTA2, Actin alpha 2; BO, Bronchiolitis obliterans; ECM, Extracellular matrix; EMT, epithelial-to-mesenchymal transition; EVG, Elastica van gieson; FFPE, Formalin fixed paraffin embedded; GO, Gene ontology; GVHD, Graft-versus-host disease; HE, hematoxylin and eosin; HSCT, Hematopoietic stem cell transplantation; MMT, Macrophage to myofibroblast transition; MRC1, Mannose receptor c-type 1; MTS, Masson's trichrome

*Correspondence and reprint requests: Nobuharu Fujii, MD, PhD, Division of Transfusion and Cell therapy, Okayama University Hospital, Okayama, Japan. 2-5-1 Shikata-cho, Kita-ku, Okayama 700-8558, Japan
E-mail address: pst33f6c@s.okayama-u.ac.jp (N. Fujii).

https://doi.org/10.1016/j.jtct.2025.12.950

Macrophage to myofibroblast transition
Myofibroblast
Spatial transcriptomics

Immunostaining showed strong co-expression of CD68, CD206, and α-SMA in foamy macrophages within and surrounding bronchioles in BO samples, with minimal expression in controls, suggesting MMT involvement. In BO, spatial transcriptomics revealed upregulation of macrophage- and TGF-β signaling genes, with distinct stage- and region-specific gene expression patterns. Unsupervised clustering revealed a shift from inflammation to fibrosis. These findings indicate that MMT contributes to fibrosis in BO. Gene expression shifts from inflammation to fibrosis as the disease advances, underscoring the importance of early intervention.

INTRODUCTION

Bronchiolitis obliterans (BO), a severe complication following hematopoietic stem cell transplantation (HSCT), is one of the primary pulmonary manifestations of chronic graft-versus-host disease (GVHD) [1,2]. BO is characterized by distinctive pathological findings, including edema and fibrosis of the bronchial walls [3,4]. The pathogenesis of BO is complex and incompletely understood [4,5] but involves a combination of inflammation, fibrosis, and airway remodeling [6,7]. The limited availability of biopsy samples, compounded by patchy distribution of BO lesions [8] and restricted access to explanted lungs from lung transplantation hinder molecular investigations of BO after HSCT.

A previous study identified macrophages within the bronchioles of human BO samples and BO model mice samples after HSCT [3,9,10], a finding we also observed demonstrating the presence of donor-derived macrophages in the bronchioles [4]. Within a single lung specimen, bronchioles at different anatomical sites exhibited varying degrees of disease progression, revealing both spatial and temporal heterogeneity in the fibrotic process, as reported in a histopathological study [8].

In BO following lung transplantation, which exhibits pathological similarities with HSCT-associated BO, macrophage-to-myofibroblast transition (MMT) has been implicated in the fibrotic process [11]. MMT has been widely documented in conditions such as pulmonary and renal fibrosis [12–14], where macrophages recruited to sites of tissue injury undergo a phenotypic shift from pro-inflammatory M1 to pro-fibrotic M2. These M2 macrophages subsequently differentiate into α-smooth muscle actin (α-SMA)-positive myofibroblasts, ultimately driving fibrosis. MMT-driven fibrosis leads to excessive production of collagen and extracellular matrix (ECM), resulting in tissue stiffening and functional impairment. This phenotypic shift in macrophages from the M1 to M2 subtype, along with fibrosis progression, has been demonstrated in our previous studies on BO following HSCT [4]. Macrophages and TGF-β are known to play central roles in the fibrotic process of BO after HSCT [15]. In addition, a recent study using organoid models of BO reported a decrease in ITGβ3, a marker associated with myofibroblast inhibition, suggesting that myofibroblasts may contribute to disease pathogenesis [16]. However, the relationship between myofibroblasts and macrophages in BO following HSCT remains unexplored.

Therefore, we aimed to investigate whether MMT contributes to the fibrotic progression of bronchiolitis obliterans following HSCT by using spatial transcriptomics.

MATERIALS AND METHODS

Patient Samples

This study was approved by the institutional review board of Okayama University (1805-003). Patient samples were obtained from cases of refractory BO following HSCT, where lung transplantation was performed as a treatment for patients aged $\geq$ 16 years between 2002 and 2022 at Okayama University Hospital, with a confirmed pathological diagnosis of BO.

Explanted lungs obtained at the time of lung transplantation were used as samples. They were from 3 patients who had acute lymphoblastic leukemia as their primary disease and developed BO 1 to 2 years after HSCT (Table 1). Uninvolved tissue from pneumonectomy specimens performed for lung cancer was used as controls (n = 2). All lung biopsy tissue samples were collected from the Department of General Thoracic Surgery and Organ Transplant Center at Okayama University Hospital. Clinical data for each patient were extracted from their medical records. Paraffin-embedded lung tissue specimens excised during the procedure were selected for analysis. In addition, commercially available normal lung specimens (VitroVivo Biotech, Rockville, MD, and Bio-Techne, Minneapolis, MN) were used as controls for immunohistochemical validation. To validate our transcriptomic findings, publicly available GeoMx DSP data (GSE255174) were processed with GeomxTools following the same pipeline used for our dataset. After quality control and normalization, both datasets were merged and batch effects were corrected.

Table 1
Characteristics of the 3 Patients With BO and 2 Patients With Lung Cancer As Controls.

Patient no.	1	2	3	4	5
Sex	F	F	M	F	F
Primary disease	ALL	ALL	ALL	Lung Cancer	Lung Cancer
Comorbidities	None	None	None	Basedow disease	Hypertension, Dyslipidemia, Type 2 diabetes mellitus
Smoke	Never	Never	Never	Past smoker; 15 cigarettes/day for 15 y	Never
Age at primary disease onset, y	13	19	16	59	84
Age at HSCT, y	18	20	18	N/R	N/R
Age at BO onset, y	19	22	19	N/R	N/R
Age at lung surgery	21	24	23	59	84
Histological stage	Middle	Early-Middle	Middle-Late	Control	Control
Donor type	MMUD	MMSD	MUR	N/R	N/R
Graft source	BM	PB	BM	N/R	N/R
Preoperative % predicted FEV_1	28.1	53.4	40.9	100.9	113.5
Preoperative FEV_1/VC	66.3	16.6	44.8	88.5	91.8
Postoperative % predicted FEV_1 (3-y follow-up)	113.1 (14 mo), 102.6 (18 mo), 98.6 (26 mo)	111.0 (6 mo), 111.0 (12 mo), 110.3 (36 mo)	112.8 (3 mo), 106.6 (6 mo)	N/R	N/R

ALL, acute lymphoblastic leukemia; MMUD, mismatched unrelated donor; MMSD, mismatched sibling donor; MUD, matched unrelated donor; N/R, not relevant.

Histopathological Evaluation

BO lesions were classified based on our previously established staging system [4] utilizing hematoxylin-eosin, Masson trichrome (MTS), and Elastica van Gleson (EVG) staining on formalin-fixed paraffin-embedded (FFPE) samples. This classification defines 3 pathological stages of BO progression:

- Early-stage: Characterized by the presence of foamy macrophages within the bronchial lumen, indicating an initial inflammatory response.
- Middle-stage: Defined by ulceration of the bronchial wall, macrophage infiltration into the bronchial epithelium, and the onset of sparse fibrosis, reflecting progressive tissue damage.
- Late-stage: Marked by bronchial lumen obstruction due to macrophage accumulation, with or without dense fibrosis, and substantial narrowing of the airways, indicating advanced fibrosis and remodeling.

To classify macrophages, CD68 (CD68 (KP1) Alexa Fluor 647, sc-20060AF647) was used as a pan-macrophage marker, and CD206 (Alexa Fluor 488 anti-human CD206 (MMR) Antibody, Cat# 32113) as an M2 marker with DAPI. Myofibroblast cells were detected using confocal laser scanning microscopy (LSM780, Carl–Zeiss) with monoclonal antibodies targeting macrophage markers and α-SMA (Alexa Fluor 594 Anti-alpha smooth muscle Actin Antibody [1A4], ab202368).

This approach enabled the detailed characterization of macrophage polarization and the identification of MMT cells within the lesions [14]. Co-staining with α-SMA, CD68, CD206, and DAPI was performed, and MMT cells were identified based on the co-expression of α-SMA with CD68 and CD206. Separate images were generated for each marker and their co-expression with α-SMA. Quantification of macrophage marker-positive cells and co-expression with α-SMA was performed using ImageJ, with cell counts recorded for each field of view. An unpaired Student's t-test was used to compare the BO and control groups.

Spatial Transcriptomics Data Generation

We analyzed lung specimens from 3 patients who developed BO following HSCT and subsequently underwent lung transplantation. Healthy lung peribronchiolar regions from 2 patients with cancer served as controls. Transcriptional profiling was conducted using the NanoString GeoMx Human Whole Transcriptome Atlas, analyzing 18,815 genes.

For fluorescence immunostaining to determine regions of interest (ROI), we used Syto13, PanCK, and CD45 from the NanoString GeoMx Solid Tumor Kit, along with CD68 (Santa Cruz, sc-20060) for staining. The lesions were reviewed and confirmed by multiple hematologists and pathologists. ROIs were selected to include foamy macrophages luminal and extraluminal the bronchioles, bronchiolar walls, alveoli, and vascular walls. Each ROI was at least 40,000 μm^3 or had a diameter of 200 to 400 μm and included approximately 200 nuclei. RNA extraction from all specimens was performed following Nanostring's protocol (https://nanostring.com/products/geomx-digital-spatial-profiler/geomx-rna-assays/geomx-whole-transcriptome-atlas/).

To ensure data quality, we applied several gene filtering steps (Supplementary Figure S1). First, the gene detection rate across samples was calculated, and genes with a detection rate below 1% were excluded from further analysis. Subsequently, each gene was evaluated for its detection frequency within individual segments, retaining only those detected in at least 10% of the segments. Finally, after these filtering criteria were applied, 10,651 genes were selected for downstream analyses. Profiling was performed on 94 ROIs across all samples.

Statistical Analysis

All analyses were performed using R software version 4.3.2 (https://cran.r-project.org) and GraphPad Prism version 9.5.1. *P*-values were calculated using 2-sided tests, with a threshold of .05 considered statistically significant.

RESULTS

Triple Co-Expression of CD68, CD206, and αSMA

First, FFPE blocks from 3 BO-diagnosed cases and 2 patients with lung cancer were stained with HE, MTS, and EVG and re-evaluated by a hematologist, thoracic surgeon, and pathologist to confirm the absence of lung cancer in the selected samples, validate the diagnosis, and assess disease stages of BO. A representative image of BO is shown in Figure 1A. Scattered fibrous structures are observed within the bronchiolar lumen, which is filled and obstructed by numerous foamy macrophages. As indicated by the arrowhead, focal thinning of the bronchiolar wall is present, with foamy macrophages found extraluminal the bronchiole, consistent with the middle phase of BO. Subsequently, we assessed the extent of co-expression of CD68, CD206, and α-SMA, characteristic markers of MMT cells, in foamy macrophages within the bronchioles (Figure 1B). The region outlined with a dashed circle represents a typical area of the co-expression of αSMA, CD68, and CD206 in BO samples. In contrast, minimal to no co-expression was observed in control samples. Quantitative analysis across the entire sample set revealed a clear trend toward increased triple-positive cells in BO samples compared to controls (Figure 1C). A similar trend was also observed in commercially available normal lung specimens used as independent controls (Supplementary Figure S2A-B). This pattern highlights the involvement of MMT cells in regions of active fibrosis in BO.

Spatial Transcriptomics Reveals Gene Differences Between BO and Control Samples

Linear mixed model analysis identified significant differential gene expression between the BO and control groups in the bronchiolar regions. Volcano plot analysis demonstrated significantly upregulated genes in the BO group compared to the control group (Figure 2A)

Notable genes included ITGB2 and IRF8, which have crucial roles in TGF-β signaling and MMT.

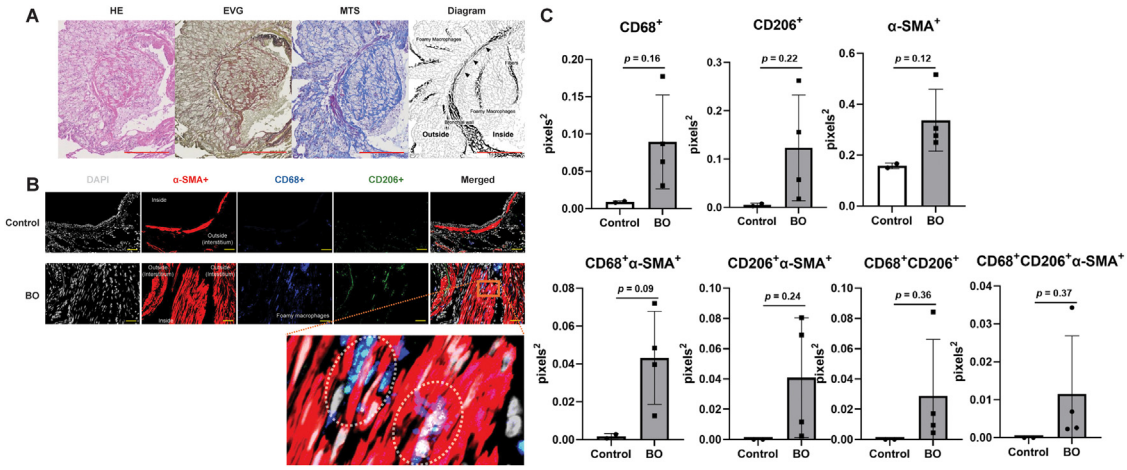

Figure 1. Pathological evidence for macrophage and myofibroblast interaction in bronchiolitis obliterans. (A) Representative pathological features of middle-phase BO in Patient 3, shown using hematoxylin and eosin (HE), Elastica van Gieson (EVG), Masson's trichrome (MTS) staining, and a diagram, presented sequentially from left to right. HE staining highlights general tissue morphology, EVG staining identifies elastic fibers, and MTS staining visualizes collagen deposition. The diagram illustrates representative histological structures in the middle phase of BO. Arrowheads indicate areas where the bronchiolar wall is destroyed, allowing foamy macrophages to spill into the extraluminal space. Scale bars = 250 μm. (B) Representative confocal microscopy images from Patient 2 (BO) and 4 (Control) showing $CD68^+$ macrophages (blue), α-smooth muscle actin (α-SMA)$^+$ myofibroblasts (red), $CD206^+$ macrophages (green), and nuclei (white). A representative area exhibiting co-expression of α-SMA, CD68, and CD206 in BO samples is highlighted by the dashed circle. Scale bars = 50 μm. (C) Comparison of single-positive cells for CD68, CD206, and alpha-smooth muscle actin, as well as co-expressing cells (BO: n = 4 lesions from 3 cases; Control: n = 2).

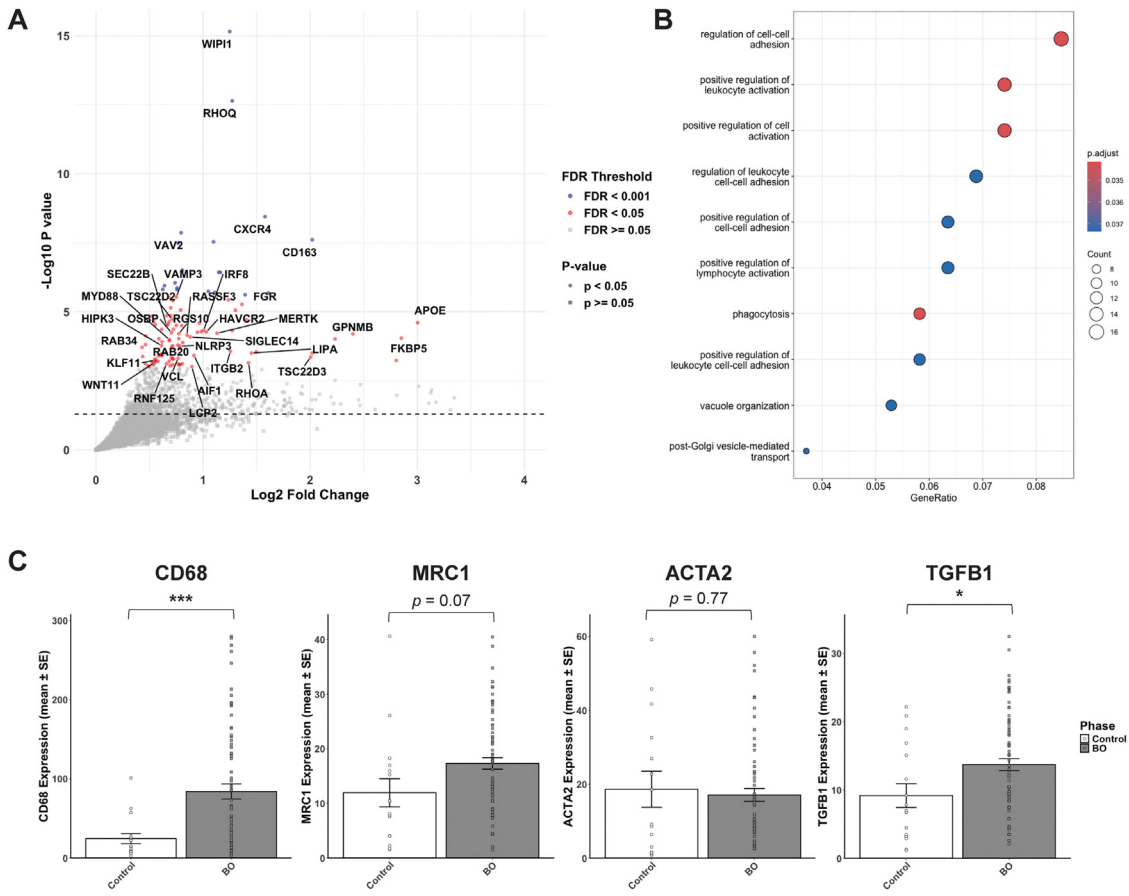

Figure 2. Comprehensive genetic analysis of bronchiolitis obliterans compared to control. (A) Volcano plot of differentially expressed genes in the bronchiolitis obliterans (BO) group. The x-axis represents the log2 fold change, while the y-axis shows the -log10 *P*-value. Genes with $P < .05$ are plotted as circles, while genes with $P \geq .05$ are displayed as squares. Significantly upregulated genes in the BO group are highlighted based on an FDR threshold of < 0.05. Specifically, genes with FDR < 0.001 are shown in red, FDR < 0.05 in blue, and FDR ≥ 0.05 in gray. The dashed line indicates the *P*-value threshold of −log10 = 1.3 (equivalent to $P = .05$). For clarity, genes with FDR < 0.05 or highly significant *P*-values (−log10 > 5) are labeled. (B) Gene Ontology (GO) enrichment analysis of significantly differentially expressed genes. Dot plot visualizing enriched biological processes identified in differentially expressed genes between the bronchiolitis obliterans and control groups. The x-axis represents the gene ratio (the proportion of significant genes associated with each term), while the y-axis lists enriched GO terms. Dot size reflects the number of genes associated with each term, and color intensity indicates statistical significance (−log10 adjusted *P*-value). (C) Bar plots depict the expression of representative macrophage-to-myofibroblast transition (MMT)-associated genes, including CD68, MRC1, ACTA2, and TGFB1, across the BO and control groups. Gene expression was analyzed using normalized data. Individual data points are displayed alongside mean ± standard error (SE) values. Error bars represent SE, and individual sample values are plotted to illustrate variability. Statistical significance was determined using t-tests for each gene. $^{*}P < .05$, $^{***}P < .001$. BO, bronchiolitis obliterans; FDR, false discovery rate; GSEA, SE; standard error, MMT; macrophage-to-myofibroblast transition

ITGB2, a β2-integrin subunit, is involved in ECM interactions and immune cell adhesion, mediating macrophage activation and tissue remodeling [17]. IRF8, a transcription factor essential for myeloid lineage differentiation, regulates macrophage polarization and has been implicated in fibrosis through its interaction with TGF-β signaling pathways [18]. In addition, CXCR4, involved in BTK and JAK1/2 signaling, regulates immune cell trafficking and inflammatory responses [19]. CD163, a macrophage-specific scavenger receptor, is linked to CSF1R signaling and plays a role in anti-inflammatory macrophage activation [20]. RHOA modulates cytoskeletal dynamics and contributes to fibrosis through the MEK/ERK, PI3K/AKT, and ROCK2 pathways [21]. Individual analyses of these genes are presented in Supplementary Figure S3A. GO enrichment analysis highlighted biological processes such as phagocytosis, positive regulation of leukocyte activation, and cell activation, indicating a close association with immune cells, particularly macrophages, which obstruct bronchioles in BO (Figure 2B). Processes such as regulation of cell-cell adhesion and post-Golgi vesicle-mediated transport were also enriched, suggesting potential roles in ECM remodeling

and fibroblast activation. Further examination of genes related to MMT showed significantly elevated expression of CD68 and TGF-β in the BO group, while MRC, the gene encoding CD206, showed a trend toward increased expression (Figure 2C). These findings collectively suggest that macrophage activation and MMT processes may contribute to the pathogenesis of BO. We compared our findings with the healthy lung samples from GSE255175 dataset and obtained consistent results. In the differential expression analysis, numerous genes exhibited concordant expression prominently in the BO group, with immune-related pathways being activated, and consistent expression patterns of CD68, MRC1, ACTA2, and TGFB1 were observed (Supplementary Figure S3B-D).

Stage-Specific and Spatial Expression Patterns of MMT-Related Markers in BO

Subsequently, we analyzed the changes in foamy macrophages across different histological stages of BO [4]. Consistent with the previous report [4], CD68 expression in foamy macrophages significantly decreased as the disease progressed (Figure 3A). A similar trend was observed for TGFB1. However, the expression of MRC1, the gene encoding CD206, and ACTA2, the gene encoding αSMA, were highest in bronchiolar extraluminal lesions during the middle phase. We further examined the correlation between CD68 and TGFB1 expression and found a strong positive correlation, with a Pearson's correlation coefficient of 0.79 ($P < .001$) and an R^2 value of 0.62 (Figure 3B). MRC1 and ACTA2 exhibited the highest levels in the middle phase compared to other disease stages. Histologically, this phase is characterized by the presence of foamy macrophages both luminal and extraluminal to the bronchioles. Given this distribution, we hypothesized that the expression of MMT-related markers might exhibit spatial specificity and analyzed differences between the luminal and extraluminal sides of the bronchioles (Figure 3C). The results showed that all MMT-related markers were more highly expressed on the extraluminal sides, suggesting a spatial distinction in marker expression between these regions.

Spatial Transcriptomics Identifies the Changes in Disease Stage Within the Foamy Macrophages in the Bronchioles

To further investigate the spatial differences in gene expression observed in the middle phase from a broader perspective, we performed an unsupervised clustering analysis focusing on MMT-related gene sets across all disease phases, incorporating spatial information (luminal/extraluminal) (Figure 4A). This analysis revealed distinct gene expression patterns between extraluminal and luminal bronchiolar lesions during the middle phase. Analysis of cell-type proportions using SpatialDecon, an R package implementing a deconvolution algorithm to estimate the relative abundance of cell types in spatial transcriptomics data, further demonstrated that macrophage distribution segregated into two distinct patterns at corresponding lesion sites (Figure 4B). We divided the samples into 2 phases based on these patterns. Linear mixed model analysis identified representative genes for each phase (Figure 4C). The earlier phase was characterized by the upregulation of TGF-β related genes, including ITGB1 [22]. LRP1, which modulates TGF-β signaling and ECM remodeling, is downregulated in fibrosis, exacerbating pro-fibrotic responses [23] PECAM1, essential for macrophage migration, facilitates leukocyte infiltration into inflamed bronchioles [24]. Other inflammatory markers included RACK1 (BTK, MEK/ERK signaling) [25], HLA-B and HLA-DPA1 (JAK1/2 signaling) [26], ITGB1 (PI3K/AKT signaling) [27], which collectively drive immune activation, adhesion, and cytoskeletal remodeling, potentially facilitating the transition from inflammation to fibrosis. Supplementary Figure S4 provides individual analyses of these genes. Finally, we performed Reactome pathway enrichment analysis across all pathways for the 2 phases. Notably, pathways indicative of TGF-β activation were prominently enriched during the earlier phase, during which MMT-related signaling pathways were also highlighted (Figure 4D). This is concordant with lung fibrosis biology in which early TGF-β activation, coupled with a macrophage M1→M2 shift, heralds subsequent fibrotic remodeling [28]. These findings support the characterization of the early to middle-extraluminal stage as the "inflammatory phase" and the middle-luminal to late stage as the "fibrotic phase" based on genomic profiling and pathological features. Subsequently, we individually evaluated representative genes associated with MMT (CD68, MRC1, ACTA2, and TGFB1) (Figure 4E). These results suggest a dynamic shift from inflammation to fibrosis within foamy macrophage-rich regions of the bronchioles, with distinct gene expression and pathway profiles characterizing each disease phase.

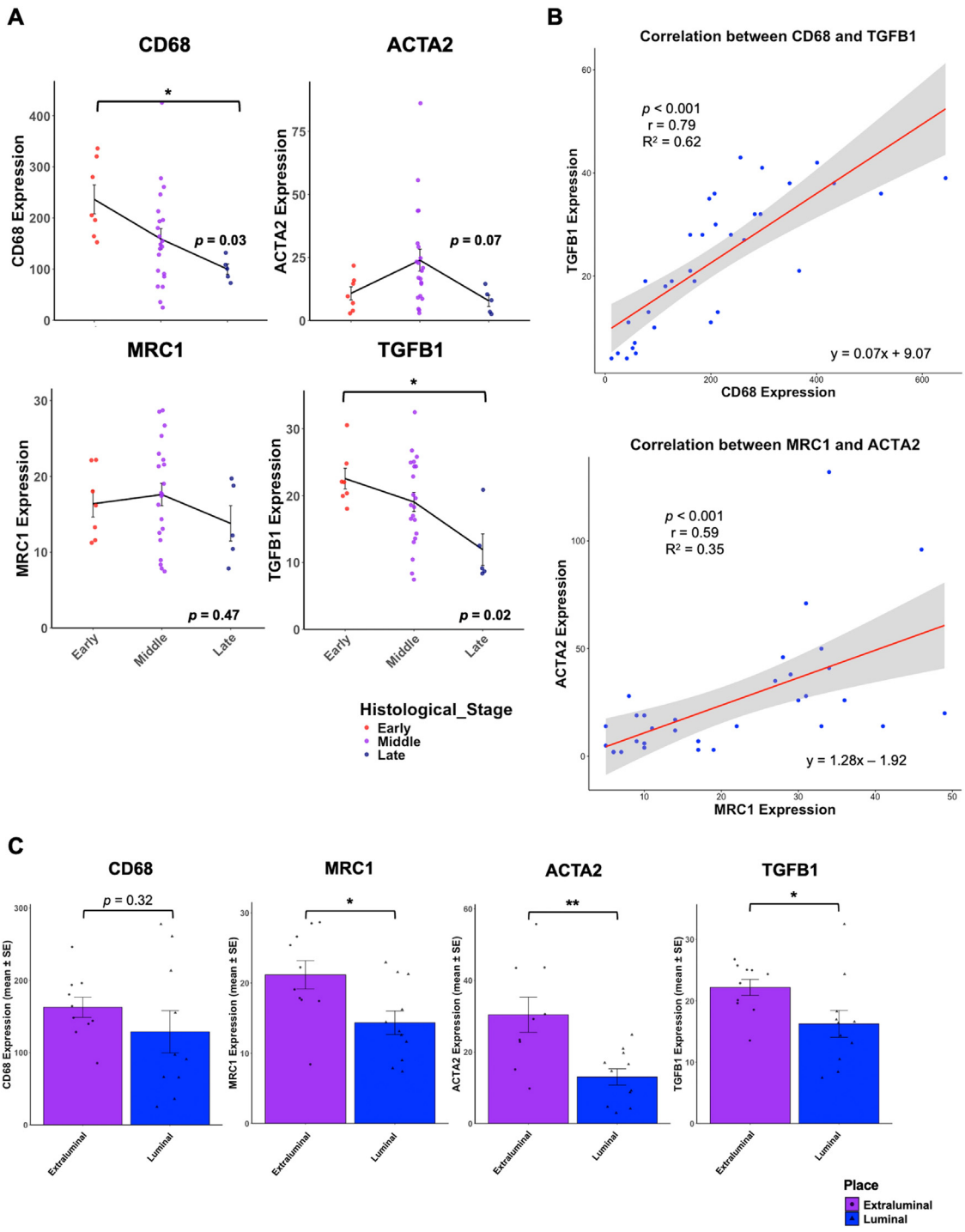

Figure 3. Gene expression patterns associated with macrophage-to-myofibroblast transition in bronchiolitis obliterans (A) Expression of selected representative genes (CD68, TGFB1, ACTA2, and MRC1) associated with macrophage-to-myofibroblast transition (MMT) across 3 histological stages (early, middle, and late). Data are presented as mean ± standard error of normalized expression values. Individual data points are shown with jitter for visualization. (B) The scatter plot illustrates the relationship between the expression of CD68 (x-axis) and TGFB1 (y-axis) in the left graph and MRC1 (x-axis) and ACTA2 (y-axis) in the right graph. Pearson's correlation coefficient is 0.79 for CD68-TGFB1 and 0.59 for MRC1-ACTA2, with both *P*-values < .001. The red line represents the linear regression fit for CD68-TGFB1 (y = 0.067x + 9.072, R^2 = 0.620) and MRC1-ACTA2 (y = 1.280x − 1.916, R^2 = 0.347). (C) Expression of selected representative genes (CD68, TGFB1, ACTA2, and MRC1) associated with macrophage-to-myofibroblast transition (MMT) was compared across different locations within the bronchioles, specifically between the luminal and extraluminal sides. The analysis focused on samples at the middle histological stage. $^{*}P < .05$, $^{**}P < .01$.

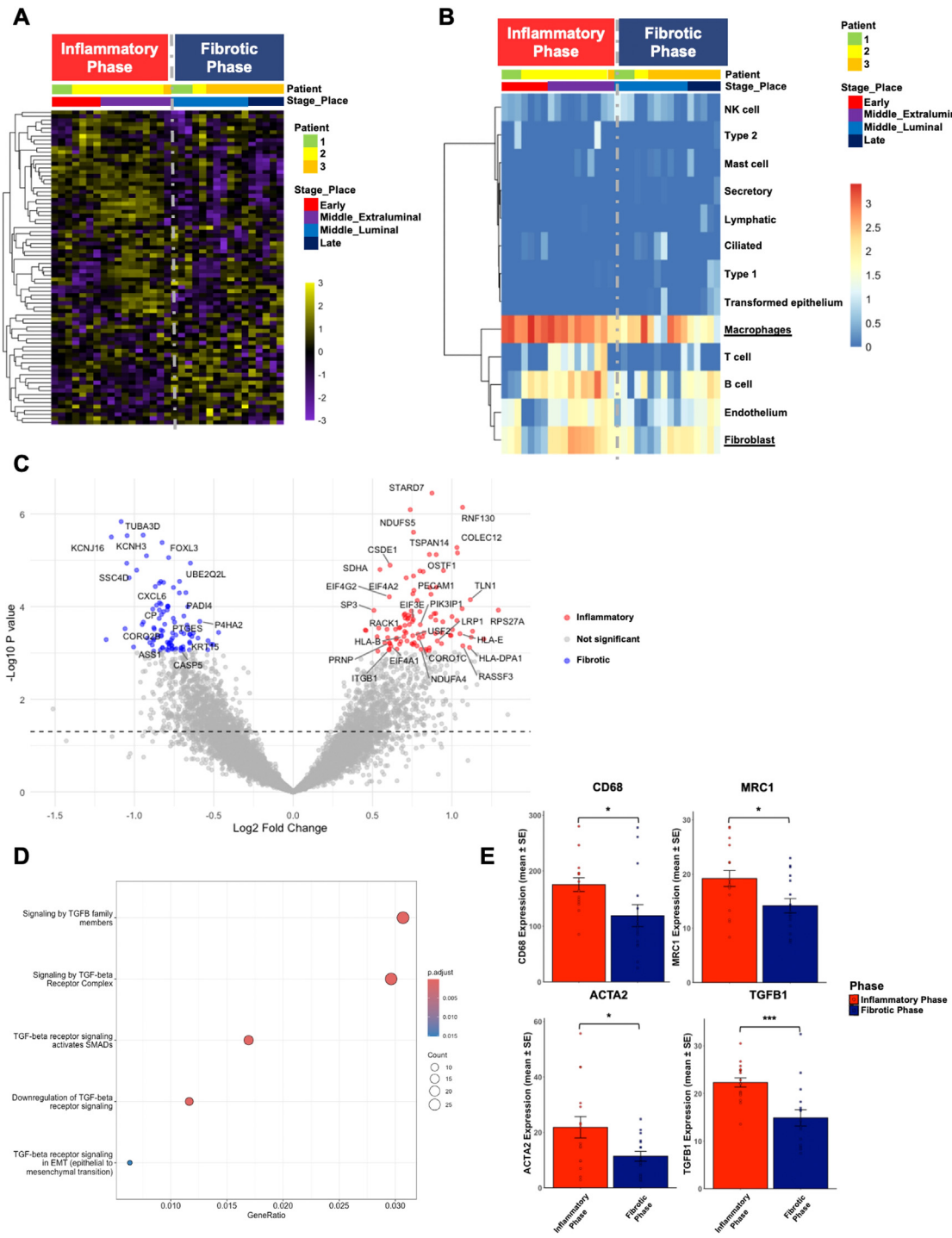

Figure 4. Transcriptional and spatial characterization of macrophage-to-myofibroblast transition (MMT) in bronchiolitis obliterans. (A) Unsupervised clustering analysis was performed to investigate gene expression patterns related to macrophage-to-myofibroblast transition (MMT). This analysis identified distinct clusters corresponding to different disease stages and lesion locations, highlighting transcriptional shifts from the inflammatory phase (early to middle extraluminal stage) to the fibrotic phase (middle luminal to late stage). (B) SpatialDecon analysis. The heatmap illustrates the results of the SpatialDecon analysis performed on normalized foamy macrophage data. Rows represent gene expression values, and columns represent individual samples sorted by disease stage, anatomical location, and patient ID. The color intensity indicates the log-transformed gene expression scores (log1p), highlighting relative differences across samples. Annotation bars at the top of the heatmap indicate the clinical attributes of each sample, including disease stage, anatomical location, and patient ID. Color coding for annotations was generated using unique hues for each category level. (C) Volcano plot of differentially expressed genes in inflammatory and fibrotic phases. The x-axis represents the log2 fold change, while the y-axis shows the −log10 *P*-value. Genes with $P < .05$ are plotted as circles, while genes with $P \geq .05$ are displayed as squares. Significantly upregulated genes in

DISCUSSION

In this study, we employed a comprehensive approach combining immunofluorescence staining and spatial transcriptomics to investigate cases of BO following HSCT. Immunofluorescence staining demonstrated a notable triple co-expression of CD68, CD206, and α-SMA in BO tissues, suggesting the involvement of MMT. Myofibroblasts can originate from various sources [14], including epithelial-mesenchymal transition (EMT) [29], endothelial-mesenchymal transition [30], proliferation of resident fibroblasts or pericytes [31], and MMT [14], but our findings highlight MMT as a key contributor to BO pathogenesis, demonstrating its contribution for the first time in this context. Spatial transcriptomics analysis marked transcriptional shifts between the inflammatory (middle-extraluminal region) and fibrotic (middle-luminal to late region) phases. Notably, M2 macrophages and α-SMA show peak expression in extraluminal lesions during the middle stage, together with other MMT-related markers, followed by a subsequent decline as fibrosis progresses. These findings collectively indicate that the pathogenesis of BO involves macrophage polarization toward an M2 phenotype, followed by differentiation into myofibroblasts, ultimately leading to fibrosis.

The TGF-β1/Smad3 signaling axis plays a central role in driving MMT [32] and therapeutic strategies targeting this pathway, such as Smad3 inhibition or blockade of upstream mediators, have shown efficacy in preclinical models [33,34]. Consistently, the antifibrotic agent pirfenidone attenuated macrophage-derived TGF-β production and ameliorated fibrosis in murine chronic GVHD, supporting the therapeutic potential of targeting TGF-β-driven pathways [10]. In addition, Src inhibition suppresses MMT and attenuates fibrosis [35], while mineralocorticoid receptor antagonists like eplerenone have demonstrated similar effects in vivo [36]. In cancer settings, targeting transcription factors such as Runx1 may also prevent MMT-derived CAF formation and tumor progression [37]. These insights highlight MMT as a potential therapeutic target in fibrotic and tumor microenvironments.

In the context of MMT, pathways upstream of the TGF-β1/Smad3 signaling axis are also being investigated as potential therapeutic targets. Recent preclinical studies in murine models of bronchiolitis obliterans have demonstrated that inhibition of BTK or CSF1R exerts antifibrotic and immunomodulatory effects, improving pulmonary function through suppression of macrophage activation and immune-mediated tissue injury [38,39]. Targeting downstream signaling pathways such as MEK/ERK and PI3K/AKT has been shown to prevent bronchiolitis development, suppress perivascular inflammation, attenuate fibrosis, and stabilize pulmonary function in similar murine models [40] Furthermore, clinical studies have reported that JAK1/2 or ROCK2 inhibitors were effective in bronchiolitis obliterans when administered at mild or early stages but showed limited efficacy in advanced disease [5,41,42], likely because foam macrophages undergo irreversible pathological and molecular changes with pathological stage progression.

The molecules that are already being explored as therapeutic targets—including JAK1, STAT3, MAPK1, PIK3IP1, CSF1R, and TGFB1—were highly expressed during the inflammatory phase in this study and showed a tendency to decrease as the pathological stage progressed. This suggests that the efficacy of inhibitors targeting these molecules may diminish in advanced stages. In human BO research analyses are often based on lung transplant specimens obtained from clinically advanced cases, as early-stage BO samples are rarely accessible in clinical practice [43]. Nevertheless, given the likelihood that clinical severity correlates with histopathological progression, as observed in other fibrotic diseases [44,45],

the BO group are highlighted based on an FDR threshold of < 0.05. Specifically, genes with FDR < 0.05 are shown in blue, and FDR ≥ 0.05 in gray. The dashed line indicates the *P*-value threshold of $-\log10 = 1.3$ (equivalent to $P = .05$). For clarity, genes with FDR < 0.05 or highly significant *P*-values ($-\log10 > 5$) are labeled. (D) Enriched Reactome pathways in the inflammatory phase compared with the fibrotic phase. Genes more highly expressed in the inflammatory phase (logFC < 0, FDR < 0.10) were subjected to Reactome pathway enrichment analysis ($P < .05$). Pathways related to TGF-β, Wnt, or Notch signaling, which are implicated in MMT pathogenesis, are highlighted. Only pathways enriched in the inflammatory phase relative to the fibrotic phase are shown. The x-axis indicates the gene ratio (proportion of input genes mapped to each pathway), while the dot color represents the adjusted *P*-value. Dot size corresponds to the number of overlapping genes within each pathway. (E) Bar plots depict the levels of representative macrophage-to-myofibroblast transition (MMT)-associated genes, including CD68, MRC1, ACTA2, and TGFB1, across the inflammatory and fibrotic phases. Gene expression was analyzed using normalized data, with individual data points displayed alongside mean ± standard error (SE) values. Error bars represent SE, and individual sample values are plotted to illustrate variability. Statistical significance was determined using t-tests for each gene. * $P < 0.05$, *** $P < 0.001$. ACTA2, Actin Alpha 2; MMT, Macrophage to myofibroblast transition; MRC1, Mannose Receptor C-type 1

therapeutic intervention targeting these inflammation-associated molecules at an early clinical stage—when inflammatory lesions are relatively predominant over fibrotic ones—appears most effective.

In addition to the importance of early intervention, future therapeutic strategies must account for the complexity of the fibrotic pathways. The inhibitors discussed above each target a single point within the cascade leading to fibrosis, including MMT, and alternative compensatory pathways may therefore limit therapeutic efficacy in BO. Although combination therapies such as pirfenidone with nintedanib in idiopathic pulmonary fibrosis [46] and ruxolitinib with belumosudil in severe chronic GVHD [47] have shown acceptable safety and modest efficacy, their benefits remain limited, underscoring the need for further investigation.

This study has some limitations. The analysis was restricted to 3 cases of lung transplantation with BO pathology from a single institution, raising concerns about selection bias and generalizability. Future studies should incorporate larger cohorts and leverage advanced spatial genomic technologies to validate these findings. Notably, these results do not clarify whether MMT is the dominant mechanism in HSCT-associated BO. As observed in lung transplant-associated BO, fibrosis through alternative pathways such as EMT may also contribute to the disease process [11,29]. Experimental studies using murine BO or organoid models to investigate TGF-β-centered pathways involved in MMT and EMT, including BTK, JAK1/2, MEK/ERK, PI3K/AKT, and ROCK2, could further elucidate their roles in the pathogenesis of BO.

In conclusion, this study demonstrates the transition of BO pathology from inflammation to fibrosis, with macrophage polarization and MMT playing central roles. Our findings provide a detailed molecular framework for the progression of BO, highlighting potential therapeutic targets in macrophage activity and tissue remodeling pathways. These insights suggest a need for stage-specific interventions to improve BO outcomes.

DATA AVAILABILITY STATEMENT

The GeoMx spatial transcriptomics data generated in this study have been deposited in the NCBI Gene Expression Omnibus (GEO) under accession number GSE316672 and will be made publicly available upon publication. The dataset is available for non-commercial research use only.

ETHICS COMMITTEE

This study was authorized by the Institutional Ethics Committee of Okayama University Hospital (IRB Permission Number: #1805-003), with opt-out consent facilitated through the hospital's website. The procedures involving human participants were conducted in compliance with the Declaration of Helsinki.

AUTHOR CONTRIBUTIONS

AY was the primary author, responsible for data collection, data analysis, and manuscript drafting. NF, KS, HF, and YM conceptualized and designed the study. NF secured funding for the study. KS, YN, YK, and DE provided technical support for GeoMx analysis, including data processing and quality control. KS, SS, YN, TN, and SK conducted histopathological evaluations and interpreted the findings. YN, TT, and HK performed statistical analyses and contributed to data interpretation. K. Fujiwara, TO, MK, TK, NA, K. Fujii, and ST contributed to result interpretation, provided critical revisions, and participated in manuscript preparation. YM supervised the entire project, oversaw manuscript development, and ensured the integrity of the research process.

ACKNOWLEDGMENT

We would like to thank the Center for Comprehensive Genomic Medicine at Okayama University Hospital and the Central Research Laboratory at Okayama University Medical School for their technical and equipment support, including assistance with the GeoMx system, sample preparation, and microscopy. We also extend our gratitude to Hirofumi Inoue of the Department of Medical Support, Okayama University Hospital, for his expertise in preparing the GeoMx tissue sections, a task requiring highly specialized technical skills.

Financial disclosure: This study was funded by the Japan Society for the Promotion of Science (JSPS) KAKENHI Grant Number 23K07627.

Conflict of Interest Statement: Takumi Kondo reports receiving research funding approximately 2.5 million JPY annually from Ono Pharmaceutical Co., Ltd. The other authors declare no conflicts of interest.

SUPPLEMENTARY MATERIALS

Supplementary material associated with this article can be found in the online version at doi:10.1016/j.jtct.2025.12.950.

REFERENCES

1. Gazourian L, Rogers AJ, Ibanga R, et al. Factors associated with bronchiolitis obliterans syndrome and chronic graft-versus-host disease after allogeneic hematopoietic cell transplantation. *Am J Hematol.*

2014;89(4):404–409. https://doi.org/10.1002/ajh.23656.
2. Baird K, Steinberg SM, Grkovic L, et al. National Institutes of Health chronic graft-versus-host disease staging in severely affected patients: organ and global scoring correlate with established indicators of disease severity and prognosis. *Biol Blood Marrow Transplant*. 2013;19(4):632–639. https://doi.org/10.1016/j.bbmt.2013.01.013.
3. Yokoi T, Hirabayashi N, Ito M, et al. Broncho-bronchiolitis obliterans as a complication of bone marrow transplantation: a clinicopathological study of eight autopsy cases. Nagoya BMT Group. *Virchows Arch*. 1997;431(4):275–282. https://doi.org/10.1007/s004280050099.
4. Kuroi T, Fujii N, Ichimura K, et al. Characterization of localized macrophages in bronchiolitis obliterans after allogeneic hematopoietic cell transplantation. *Int J Hematol*. 2021;114(6):701–708. https://doi.org/10.1007/s12185-021-03214-7.
5. Zhao Y, OuYang G, Shi J, et al. Salvage therapy with low-dose ruxolitinib leads to a significant improvement in bronchiolitis obliterans syndrome in patients with CGVHD after allogeneic hematopoietic stem cell transplantation. *Front Pharmacol*. 2021;12:668825. https://doi.org/10.3389/fphar.2021.668825.
6. Pham J, Rangaswamy J, Avery S, et al. Updated prevalence, predictors and treatment outcomes for bronchiolitis obliterans syndrome after allogeneic stem cell transplantation. *Respiratory Medicine*. 2021;177:106286. https://doi.org/10.1016/j.rmed.2020.106286.
7. Chen S, Zhao K, Lin R, et al. The efficacy of mesenchymal stem cells in bronchiolitis obliterans syndrome after allogeneic HSCT: A multicenter prospective cohort study. *eBioMedicine*. 2019;49:213–222. https://doi.org/10.1016/j.ebiom.2019.09.039.
8. Meignin V, Thivolet-Bejui F, Kambouchner M, et al. Lung histopathology of non-infectious pulmonary complications after allogeneic haematopoietic stem cell transplantation. *Histopathology*. 2018;73(5):832–842. https://doi.org/10.1111/his.13697.
9. Panoskaltsis-Mortari A, Tram KV, Price AP, Wendt CH, Blazar BR. A new murine model for bronchiolitis obliterans post-bone marrow transplant. *Am J Respir Crit Care Med*. 2007;176(7):713–723. https://doi.org/10.1164/rccm.200702-335OC.
10. Du J, Paz K, Flynn R, et al. Pirfenidone ameliorates murine chronic GVHD through inhibition of macrophage infiltration and TGF-β production. *Blood*. 2017;129(18):2570–2580. https://doi.org/10.1182/blood-2017-01-758854.
11. Campli M-PD, Azouz A, Assabban A, et al. The mononuclear phagocyte system contributes to fibrosis in post-transplant obliterans bronchiolitis. *Eur Respir J*. 2021;57(3):2000344. https://doi.org/10.1183/13993003.00344-2020.
12. Meng XM, Wang S, Huang XR, et al. Inflammatory macrophages can transdifferentiate into myofibroblasts during renal fibrosis. *Cell Death Dis*. 2016;7(12):e2495. https://doi.org/10.1038/cddis.2016.402.
13. Chen X, Tang J, Shuai W, Meng J, Feng J, Han Z. Macrophage polarization and its role in the pathogenesis of acute lung injury/acute respiratory distress syndrome. *Inflamm Res*. 2020;69(9):883–895. https://doi.org/10.1007/s00011-020-01378-2.
14. Li X, Liu Y, Tang Y, Xia Z. Transformation of macrophages into myofibroblasts in fibrosis-related diseases: emerging biological concepts and potential mechanism. *Front Immunol*. 2024;15:1474688. https://doi.org/10.3389/fimmu.2024.1474688.
15. Zeiser R, Blazar BR. Pathophysiology of chronic graft-versus-host disease and therapeutic targets. *N Engl J Med*. 2017;377(26):2565–2579. https://doi.org/10.1056/NEJMra1703472.
16. Lee J, Venapally A, Maekawa R, Takayama S, Williams KM. Human lung organoid model of bronchiolitis obliterans syndrome following hematopoietic cell transplantation. *Blood*. 2024;144(Supplement 1):4768. https://doi.org/10.1182/blood-2024-203791.
17. Hoffmann EJ, Ponik SM. Biomechanical contributions to macrophage activation in the tumor microenvironment. *Front Oncol*. 2020;10:787. https://doi.org/10.3389/fonc.2020.00787.
18. Humblin E, Thibaudin M, Chalmin F, et al. IRF8-dependent molecular complexes control the Th9 transcriptional program. *Nat Commun*. 2017;8(1):2085. https://doi.org/10.1038/s41467-017-01070-w.
19. Montresor A, Toffali L, Rigo A, Ferrarini I, Vinante F, Laudanna C. CXCR4- and BCR-triggered integrin activation in B-cell chronic lymphocytic leukemia cells depends on JAK2-activated Bruton's tyrosine kinase. *Oncotarget*. 2018;9(80):35123–35140. https://doi.org/10.18632/oncotarget.26212.
20. Moestrup SK, Møller HJ. CD163: a regulated hemoglobin scavenger receptor with a role in the anti-inflammatory response. *Ann Med*. 2004;36(5):347–354. https://doi.org/10.1080/07853890410033171.
21. Bei Y, Hua-Huy T, Nicco C, et al. RhoA/Rho-kinase activation promotes lung fibrosis in an animal model of systemic sclerosis. *Exp Lung Res*. 2016;42(1):44–55. https://doi.org/10.3109/01902148.2016.1141263.
22. Reed NI, Jo H, Chen C, et al. The $\alpha v\beta 1$ integrin plays a critical in vivo role in tissue fibrosis. *Sci Transl Med*. 2015;7(288):288ra279. https://doi.org/10.1126/scitranslmed.aaa5094.
23. Schnieder J, Mamazhakypov A, Birnhuber A, et al. Loss of LRP1 promotes acquisition of contractile-myofibroblast phenotype and release of active TGF-β1 from ECM stores. *Matrix Biol*. 2020;88:69–88. https://doi.org/10.1016/j.matbio.2019.12.001.
24. Sugimoto N, Rui T, Yang M, et al. Points of control exerted along the macrophage-endothelial cell-polymorphonuclear neutrophil axis by PECAM-1 in the innate immune response of acute colonic inflammation1. *J Immunol*. 2008;181(3):2145–2154. https://doi.org/10.4049/jimmunol.181.3.2145.
25. Pu Y, Wu Y, Zhou Y, Wan L-H. Azithromycin suppresses TGF-β1-related epithelial-mesenchymal transition in airway epithelial cells via targeting RACK1. *Chemico-Biol Interactions*. 2023;370:110332. https://doi.org/10.1016/j.cbi.2022.110332.
26. Khatri A, Todd JL, Kelly FL, et al. JAK-STAT activation contributes to cytotoxic T cell-mediated basal cell death in human chronic lung allograft dysfunction. *JCI Insight*. 2023;8(6). https://doi.org/10.1172/jci.insight.167082.
27. Bi Z, Zang G, Wang X, Tian L, Zhang W. Integrins and pulmonary fibrosis: Pathogenic roles and therapeutic opportunities. *Biomol Biomed*. 2025;26(2):200–214. https://doi.org/10.17305/bb.2025.12545.
28. Kamiya M, Carter H, Espindola MS, et al. Immune mechanisms in fibrotic interstitial lung disease. *Cell*. 2024;187(14):3506–3530. https://doi.org/10.1016/j.cell.2024.05.015.
29. Borthwick LA, Parker SM, Brougham KA, et al. Epithelial to mesenchymal transition (EMT) and airway

remodelling after human lung transplantation. *Thorax*. 2009;64(9):770–777. https://doi.org/10.1136/thx.2008.104133.
30. Ng YY, Huang TP, Yang WC, et al. Tubular epithelial-myofibroblast transdifferentiation in progressive tubulointerstitial fibrosis in 5/6 nephrectomized rats. *Kidney Int*. 1998;54(3):864–876. https://doi.org/10.1046/j.1523-1755.1998.00076.x.
31. Zeisberg EM, Tarnavski O, Zeisberg M, et al. Endothelial-to-mesenchymal transition contributes to cardiac fibrosis. *Nat Med*. 2007;13(8):952–961. https://doi.org/10.1038/nm1613.
32. Wang S, Meng XM, Ng YY, et al. TGF-β/Smad3 signalling regulates the transition of bone marrow-derived macrophages into myofibroblasts during tissue fibrosis. *Oncotarget*. 2016;7(8):8809–8822. https://doi.org/10.18632/oncotarget.6604.
33. Meng XM, Huang XR, Chung AC, et al. Smad2 protects against TGF-beta/Smad3-mediated renal fibrosis. *J Am Soc Nephrol*. 2010;21(9):1477–1487. https://doi.org/10.1681/asn.2009121244.
34. Lan HY, Chung AC. TGF-β/Smad signaling in kidney disease. *Semin Nephrol*. 2012;32(3):236–243. https://doi.org/10.1016/j.semnephrol.2012.04.002.
35. Tang PM, Zhou S, Li CJ, et al. The proto-oncogene tyrosine protein kinase Src is essential for macrophage-myofibroblast transition during renal scarring. *Kidney Int*. 2018;93(1):173–187. https://doi.org/10.1016/j.kint.2017.07.026.
36. Xiong Y, Chang Y, Hao J, et al. Eplerenone attenuates fibrosis in the contralateral kidney of UUO rats by preventing macrophage-to-myofibroblast transition. *Front Pharmacol*. 2021;12:620433. https://doi.org/10.3389/fphar.2021.620433.
37. Tang PC, Chan MK, Chung JY, et al. Hematopoietic Transcription Factor RUNX1 is Essential for Promoting Macrophage-Myofibroblast Transition in Non-Small-Cell Lung Carcinoma. *Adv Sci (Weinh)*. 2024;11(1):e2302203. https://doi.org/10.1002/advs.202302203.
38. Dubovsky JA, Flynn R, Du J, et al. Ibrutinib treatment ameliorates murine chronic graft-versus-host disease. *J Clin Invest*. 2014;124(11):4867–4876. https://doi.org/10.1172/jci75328.
39. Alexander KA, Flynn R, Lineburg KE, et al. CSF-1-dependant donor-derived macrophages mediate chronic graft-versus-host disease. *J Clin Invest*. 2014;124(10):4266–4280. https://doi.org/10.1172/jci75935.
40. Muranushi H, Shindo T, Chen-Yoshikawa TF, et al. Dual inhibition of the MEK/ERK and PI3K/AKT pathways prevents pulmonary GVHD suppressing perivenulitis and bronchiolitis. *Blood Advances*. 2023;7(1):106–121. https://doi.org/10.1182/bloodadvances.2021006678.
41. Kambara Y, Fujii N, Usui Y, et al. Association between early corticosteroid administration and long-term survival in non-infectious pulmonary complications after allogeneic hematopoietic stem cell transplantation. *Int J Hematol*. 2023;117(4):578–589. https://doi.org/10.1007/s12185-022-03517-3.
42. DeFilipp Z, Kim HT, Yang Z, et al. Clinical response to belumosudil in bronchiolitis obliterans syndrome: a combined analysis from 2 prospective trials. *Blood Adv*. 2022;6(24):6263–6270. https://doi.org/10.1182/bloodadvances.2022008095.
43. Estenne M, Hertz MI. Bronchiolitis obliterans after human lung transplantation. *Am J Respir Crit Care Med*. 2002;166(4):440–444. https://doi.org/10.1164/rccm.200201-003pp.
44. Pandiar D, Priyadarshini G, Poothakulath Krishnan R, Uma Maheswari T N. Correlation between clinical and histopathological stagings of oral submucous fibrosis: a clinicopathological cognizance of 238 cases from South India. *Cureus*. 2023;15(11):e49107. https://doi.org/10.7759/cureus.49107.
45. Kim MY, Cho MY, Baik SK, et al. Histological subclassification of cirrhosis using the Laennec fibrosis scoring system correlates with clinical stage and grade of portal hypertension. *J Hepatol*. 2011;55(5):1004–1009. https://doi.org/10.1016/j.jhep.2011.02.012.
46. Huh JY, Lee JH, Song JW. Efficacy and safety of combination therapy with pirfenidone and nintedanib in patients with idiopathic pulmonary fibrosis. *Front Pharmacol*. 2023;14:1301923. https://doi.org/10.3389/fphar.2023.1301923.
47. Caputo J, Peddireddi A, Wall SA, et al. Axatilimab Combination therapies with ruxolitinib and/or belumosudil induces clinical responses in patients with severe, treatment-refractory chronic Gvhd. *Transplant Cell Therapy, Official Publication Am Soc Transplant Cell Therapy*. 2025;31(2):S82–S83. https://doi.org/10.1016/j.jtct.2025.01.132.